

Article

Quantum Interference Effects on Josephson Current through Quadruple-Quantum-Dot Molecular Inserted between Superconductors

Yumei Gao ¹, Yaohong Shen ², Feng Chi ^{1,*}, Zichuan Yi ¹  and Liming Liu ¹

¹ School of Electronic and Information Engineering, UEST of China, Zhongshan Institute, Zhongshan 528400, China; yumeigao@zsc.edu.cn (Y.G.); yizichuan@zsc.edu.cn (Z.Y.); liulmxps@zsc.edu.cn (L.L.)

² South China Academy of Advanced Optoelectronics, South China Normal University, Guangzhou 510006, China; 2023024194@m.scnu.edu.cn

* Correspondence: chifeng@semi.ac.cn

Abstract: We study theoretically the Josephson current through a junction composed of quadruple quantum dots (QDs), of which only one is coupled directly to the left and right superconductor leads (denoted by QD1). The other three QDs are side-coupled to QD1 and free from coupling to the leads. It is found that when the energy levels of all the four QDs are identical, the Josephson current varying with energy level of QD1 develops three peaks with two narrow and one wide, showing the typical Dicke lineshape. With increasing inter-dot coupling strength, the triple-peak configuration is well retained and accompanied by an obviously increased current amplitude. The critical current as a function of the energy level of QD1 shows a single resonance peak whose position and height depend on the energy levels of the side-coupled QDs and the inter-dot coupling strengths. We also find that the curve of the critical current versus energy levels of the side-coupled QDs shows a pair of Fano resonances and the same number Fano antiresonances (valleys). When the energy levels of the side-coupled QDs are different from each other, another Fano resonance and antiresonance are induced due to the quantum interference effect. The present results are compared with those in double and triple QDs systems, and may serve as unique means, such as the combination of quantum Dicke and Fano effects, to manipulate the Josephson currents.

Keywords: Josephson effect; critical Josephson current; quadruple quantum dots; Dicke effect; Fano effect



Citation: Gao, Y.; Shen, Y.; Chi, F.; Yi, Z.; Liu, L. Quantum Interference Effects on Josephson Current through Quadruple-Quantum-Dot Molecular Inserted between Superconductors.

Micromachines **2024**, *15*, 1225. <https://doi.org/10.3390/mi15101225>

Academic Editor: Ai-Qun Liu

Received: 26 August 2024

Revised: 23 September 2024

Accepted: 24 September 2024

Published: 30 September 2024



Copyright: © 2024 by the authors. Licensee MDPI, Basel, Switzerland. This article is an open access article distributed under the terms and conditions of the Creative Commons Attribution (CC BY) license (<https://creativecommons.org/licenses/by/4.0/>).

1. Introduction

It was predicted theoretically by B.D. Josephson that Cooper pairs will carry tunnel currents from one superconductor to another through an ultra-thin insulating layer [1]. This phenomenon was subsequently named as the Josephson effect and the associated tunnel currents are the Josephson current or supercurrent. It paved the way for the study of a series of interesting phenomena and diverse applications due to the coherent flow of Cooper-pair currents [2,3]. The development of superconducting devices based on the Josephson effect is determined by two tightly connected aspects of materials science and nanotechnologies related to superconductivity. Advances in materials science brings about not only new superconductors, and novel capabilities in designing interfaces and growing heterostructure under precise control. Progresses in nanotechnologies for superconductivity offer new experimental tools to build completely new families of devices. From a material point of view, the superconductors in tunnel Josephson junctions underwent a change from the early soft superconductors, such as Sn and In, to the more mature class of devices based on rigid superconductors, such as Nb [2–4], and to superconductors driven into topological states in recent years [3–5]. Along with the exploration of the superconductors, new barriers

or layers were also introduced to replace the original insulator layer with high resistance, including the more transmissive metallic, semiconductor and ferromagnetic barriers [4,6]. These hybridized systems induce novel physical processes due to the proximity effect from a mutual influence of a superconductor in contact with these barriers, such as the Andreev reflection that converts a dissipative electrical current into dissipationless supercurrent at an interface between the superconductor and normal metallic layer.

In devices composed of superconductors hybridized with semiconductors, interface effects and boundary conditions will exert significant impacts on the proximity effect and the coherent transport processes from the leads to the barrier [3,6]. The coherence length in the semiconductor barrier depends on the Cooper pair density through the diffusion constant and can be adjusted by a gate voltage. These barriers are generally fabricated in two-dimensional electron gas (2DEG) systems, from which the zero-dimensional semiconductor quantum dots (QDs) can be defined [7,8]. Interests in electronic tunneling through QDs were intrigued by the observation of phenomena like the Coulomb blockade effect since the early 1990s [9]. It was soon discovered that QDs could offer an ideal platform for studying more subtle transport processes of basic electronic correlations phenomena like the Kondo effect [10,11]. A great advantage of QD-based devices is to control the relevant parameters, and enable a direct comparison of observed experimental results with the theoretical predictions. With the development of mesoscopic physics, a more detailed investigation on transport through single-level QD inserted between superconductors was carried out focusing on the concept of coherent Andreev reflection [7,12–21]. In such systems, the spectral density of states is characterized by the presence of the Andreev bound states (ABSs) formed within the superconductor gap. They are sensitive to the phase difference between the superconductors and are usually the dominant contribution to the Josephson current.

In recent years, there has been a growing interest in systems with multiple QDs or several quantum channels in a single QD [7]. These multidot systems could allow for the study of non-local electronic transport, quantum interference effect and the possibility of creating entangled electron pairs with the help of crossed or non-local Andreev processes. The Josephson effect through systems composed of double QDs arranged in either parallel or series to superconductor leads has been extensively studied theoretically and experimentally [22–29]. It was found that the Josephson current can be fully manipulated by adjusting the hybridization between the dots, symmetry or the spin states of the devices [30–32]. In the presence of spin orbit interaction, positive and negative critical Josephson currents may be different from each other, resulting in the interesting Josephson diode effect that has aroused much recent attention [18,33]. There is also some recent work concerning the Josephson effect in triple-quantum-dots (TQDs) systems. It was found the mutual competition and cooperation of Cooper-pair correlation and Kondo correlation will result in $0 - \pi$ transition behaviors of the Josephson current by controlling the inter-dot couplings [34]. The quantum Dicke effect will induce new peak around the Fermi energy levels of the superconductors coupled to TQDs arranged in cross-typed configuration [35]. In closed ring-shape TQDs with superconductor leads, it was found that the sign change and phase transition can be adjusted by the quantum interference effect [36–39].

In the present manuscript, we study the Josephson effect in a quadruple QDs molecule inserted between superconductor leads as shown in Figure 1. In previous work [40], this device has been proposed to function as a spin-filter, as well as to enhance the Seebeck coefficient by tuning the energy levels of the QDs. Here we find that when the QDs molecule is connected to superconductor leads, the interesting quantum interference effect will change the Josephson current significantly. For example, the Josephson current varying with respect to the energy level of QD1 shows a triple-peak configuration exhibiting the Dicke effect characterized by different peaks' widths [35,41–45]. As for the critical current, which is the maximum of Josephson current in a 2π period of the phase difference between the superconductors, there is a single resonant peak when it is varied with the energy level of QD1. Different from a the double- or triple-QDs system [25,35], the peak's position can

be changed from positive QD1 energy level to a negative one or vice versa by changing the energy level of the side-coupled QDs or the inter-dot coupling strength. The critical current shows Fano line-shape characterized by asymmetric resonance and valley in the curve varying with respect to the energy level of the side-coupled QDs. When the energy levels of the side-coupled QDs are the same, there are two Fano resonances and the accompanied by two valleys. Another Fano resonance and valley emerge when the energy levels of the side-coupled QDs are different from each other, which is quite different from the results in double- or triple-QDs structures. The QDs in the present structure can be realized by applying gate voltages on 2DEGs defined such as in GaAs/AlGaAs heterostructures. By changing the gate voltages, the strengths and directions of the confining potentials on the 2DEGs can be adjusted, so as to control the energy levels of the QDs. Moreover, it may also change the present multiple QDs into other interesting constrictions such as quantum point contacts [46].

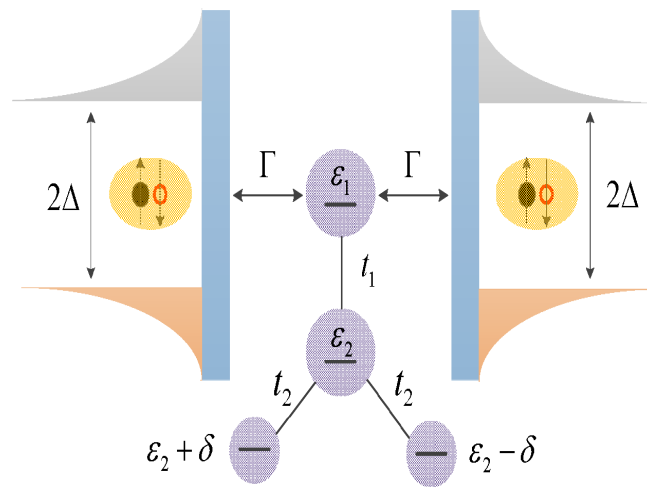


Figure 1. The schematic diagram of the quadruple quantum dots sandwiched between the left and right superconductors with energy gap Δ . Only quantum dot 1 with energy level ε_1 couples directly to the superconductors with a strength of Γ , and interacts simultaneously with quantum dot 2 with energy level ε_2 by coupling strength t_1 . Quantum dot 2 is further connected to quantum dots 3 and 4 individually having energy levels $\varepsilon_2 + \delta$ $\varepsilon_2 - \delta$ by the same coupling strength t_2 .

2. Model and Method

The proposed Josephson junction consists of quadruple QDs of which only one is coupled to the superconductor leads, as shown in Figure 1. We assume that there is only one energy level in each QD and neglect the Coulomb interaction between electrons, which is similar to the case in refs. [12–14]. This is because that the Coulomb interaction will not change the main results of the present paper obtained at zero temperature, especially the quantum interference effects on the Josephson current [18,22–25]. In experiments, it is also possible to enable only one energy level on the QD to locate between the transport window by applying a strong enough vertical magnetic field on the dots [47]. The structure’s Hamiltonian is divided into three parts as $H = H_{QDs} + H_{leads} + H_T$ [13,15,40], in which the Hamiltonian of the QDs and interaction between them is

$$H_{QDs} = \sum_{i=1,\sigma}^4 \varepsilon_i d_{i\sigma}^\dagger d_{i\sigma} + t_1 \sum_{\sigma} (d_{1\sigma}^\dagger d_{2\sigma} + \text{H.c.}) + t_2 \sum_{\sigma} (d_{2\sigma}^\dagger d_{3\sigma} + d_{2\sigma}^\dagger d_{4\sigma} + \text{H.c.}), \quad (1)$$

where the creation (annihilation) operator $d_{i\sigma}^\dagger$ ($d_{i\sigma}$) is for electrons in the i -th QD with energy level ε_i and spin state σ . The dots’ energy levels ε_i can be adjusted experimentally by gate voltages V_g . The QD1 is coupled by tunnel junction to QD2 with a strength of t_1 , and QD2 couples simultaneously to QDs 3 and 4 with the same strength t_2 . The energy

level of QD3(4) is set to be $\varepsilon_{3(4)} = \varepsilon_2 + (-)\delta$. The Hamiltonian H_{leads} stands for the two superconductors, and is given by [13,15],

$$H_{leads} = \sum_{\alpha,k,\sigma} \varepsilon_{\alpha,k\sigma} C_{\alpha,k\sigma}^\dagger C_{\alpha,k\sigma} + \sum_{\alpha,k} (\Delta_\alpha e^{i\phi_\alpha} C_{\alpha,k\uparrow}^\dagger C_{\alpha,-k\downarrow} + \text{H.c.}) \quad (2)$$

where $C_{\alpha,k\sigma}^\dagger$ ($C_{\alpha,k\sigma}$) is the creation (annihilation) operator of the electron in lead α ($\alpha = L, R$) with energy $\varepsilon_{\alpha,k\sigma}$, superconducting energy gap Δ_α and phase ϕ_α . The Josephson current arises from the phase bias $\phi = \phi_L - \phi_R$ in the absence of external bias voltage. The Hamiltonian H_T is for the tunneling between the QD1 and the leads,

$$H_T = \sum_{\alpha,k,\sigma} (t_\alpha C_{\alpha,k\sigma}^\dagger d_{1\sigma} + \text{H.c.}) \quad (3)$$

where t_α is the coupling strength between QD1 and lead- α .

The Josephson current J , which is contributed from transport processes of Andreev reflection, crossed Andreev reflection and single electron tunneling [48,49], is calculated by adopting the nonequilibrium Green's function method. In the standard Nambu representation $\psi_i = (d_{i\uparrow}^\dagger, d_{i\downarrow})^\dagger$ and $\psi_\alpha = (C_{\alpha,k\uparrow}^\dagger, C_{\alpha,-k\downarrow})^\dagger$, the explicit expression for J is given as follows, [13,14,19]

$$J = J_\uparrow + J_\downarrow = \frac{2e}{\hbar} \int d\varepsilon \text{ReTr} \{ \sigma_z [\mathbf{G}_d^a (\Sigma_L^a - \Sigma_R^a) - \mathbf{G}_d^r (\Sigma_L^r - \Sigma_R^r)] \} f(\varepsilon), \quad (4)$$

where $\sigma_z = \text{diag}(1, -1)$, and $\mathbf{G}_d^{r/a}$ is the retarded/advanced Green's function of QD1. The quantity $\Sigma_{L/R}^{r/a}$ is the retarded/advanced self-energy contributed from the left/right superconductor lead, and $f(\varepsilon) = 1/[1 + \exp(\varepsilon/k_B T)]$ is the equilibrium Dirac Fermi function with T and k_B as the temperature and Boltzmann constant, respectively. The retarded/advanced Green's function $\mathbf{G}_d^{r/a}$ is calculated using the equation of motion method. After some straightforward processes, \mathbf{G}_d^r is obtained in the Dyson equation form [13,14,19,25,40],

$$\mathbf{G}^r = \mathbf{g}^r + \mathbf{g}^r \Sigma^r \mathbf{G}^r, \quad (5)$$

in which \mathbf{g}^r is the retarded Green's function of QD1 coupling to the other QDs in the absence of interaction between the superconductors, which is taken into consideration by introducing the self-energy Σ^r . The 2×2 matrix \mathbf{g}^r is given by [13,14,19,25,40],

$$\mathbf{g}^r = \begin{bmatrix} \varepsilon - \varepsilon_1 - \Sigma_{QDs,-}^{r/a} + i0^+ & 0 \\ 0 & \varepsilon + \varepsilon_1 - \Sigma_{QDs,+}^{r/a} + i0^+ \end{bmatrix}^{-1}, \quad (6)$$

in which the self-energy contributed from QDs 2, 3 and 4 is given by [40],

$$\Sigma_{QDs,\pm}^r = \frac{t_1^2}{\varepsilon \pm \varepsilon_2 - \frac{t_2^2}{\varepsilon \pm \varepsilon_2 \pm \delta + i0^+} - \frac{t_2^2}{\varepsilon \pm \varepsilon_2 \mp \delta + i0^+} + i0^+}. \quad (7)$$

The retarded self-energy contributed from the superconductor leads are [13,14,25],

$$\Sigma_\alpha^r = -\frac{i}{2} \Gamma_\alpha \gamma_\alpha(\varepsilon) \begin{bmatrix} 1 & -\frac{\Delta_\alpha}{\varepsilon} e^{-i\phi_\alpha} \\ -\frac{\Delta_\alpha}{\varepsilon} e^{i\phi_\alpha} & 1 \end{bmatrix}, \quad (8)$$

with $\gamma_\alpha(\varepsilon)$ being the density of states of the superconductor [13],

$$\gamma_\alpha(\varepsilon) = \frac{|\varepsilon|\vartheta(|\varepsilon| - \Delta_\alpha)}{\sqrt{\varepsilon^2 - \Delta_\alpha^2}} + \frac{\varepsilon\vartheta(\Delta_\alpha - |\varepsilon|)}{i\sqrt{\Delta_\alpha^2 - \varepsilon^2}}, \quad (9)$$

in which $\vartheta(x) = 1$ for $x > 0$ and $\vartheta(x) = 0$ otherwise. The advanced self-energy and Green's function are $\Sigma_\alpha^a = \Sigma_\alpha^{r+}$, and $\mathbf{G}^a = \mathbf{G}^{r+}$. Under the wide-band approximation, the line-width function in Equation (8) is $\Gamma_\alpha = 2\pi t_\alpha^2 \rho_\alpha$, is ρ_α the normal density of states in lead- α .

3. Numerical Results

Here, we consider that the two superconductor leads are made of the same material and set $\Delta_L = \Delta_R = \Delta$, which is fixed at $\Delta \equiv 1$, as the energy unit. The phase factors of the leads are chosen as $\phi_L = -\phi_R = \phi/2$. We also assume that QD1 is weakly coupled to the superconductors with symmetrical strength, $\Gamma_L = \Gamma_R = 0.1\Delta$. All the calculations are performed at zero temperature $T = 0$ with the constants $e = k_B = h = 1$. The Josephson current is measured in unit of $J_0 = e\Delta/\hbar$ throughout the manuscript.

3.1. Identical Dots' Levels: $\varepsilon_1 = \varepsilon_2 = \varepsilon_0, \delta = 0$

Figure 2 presents the Josephson current under the conditions of identical dots' energy levels and equal inter-dot coupling strengths ($t_1 = t_2 = t_0$). Figure 2a shows that the Josephson current J is a 2π -periodic function of the phase bias ϕ , and is antisymmetrical with respect to $\phi = \pi$, i.e., $J(\phi) = -J(\phi + \pi)$, showing the typical Josephson effect [1,3,13,50]. In fact, such a property of the Josephson current remains unchanged throughout the present manuscript regardless of the values of the dots' energy levels, coupling strengths between the QDs, and the detuning of the dots' levels. For a fixed value of ϕ except for $\phi = n\pi$ ($n = 0, 1, 2, \dots$), there are three current peak in the curve of $J \sim \varepsilon_0$. The peaks' positions can be determined by setting the denominator of the free Green's function of QD1 in Equation (6) to be zero. After some straightforward calculations, one finds that the current develops peaks at $\varepsilon_0 = 0$ (double degenerate), and $\varepsilon_{0,\pm} = \pm\sqrt{3}t_0$ under these completely symmetrical conditions. Moreover, the central peak at $\varepsilon_0 = 0$ is wider and higher than those at $\pm\sqrt{3}t_0$ due to the Dicke effect found previously in multiple QDs structures [35,36,38]. The present triple-peak configuration in J is similar to the vertical three-QD structure [35], in which the peaks are at $\varepsilon_0 = 0$, and $\pm\sqrt{2}t_0$, respectively. Figure 2b presents J varying with respect to ε_0 and t_0 for fixed $\phi = \pi/2$. When QD1 is decoupled from the other QDs, i.e., $t_0 = 0$, the current J shows the typical single-peak configuration centered at $\varepsilon_0 = 0$. Turning on the inter-dot couplings ($t_0 \neq 0$), the current shows the triple-peak configuration with a slight reduction in the central peak. Notice that, again, the triple-peak configuration in this quadruple QDs structure is quite different from that of the three-QD one, in which the central peak is very low [35].

Figure 3 shows the impacts of t_2 and δ on the Josephson current J varying as a function of ϕ . For the case of $t_1 = 0.3$ and $t_2 = 0$, the present structure consists of two QDs, and the maximum of J is about $0.06J_0$ as indicated by the solid line in Figure 3a. When QD1 is coupled to the side-coupled QDs ($t_2 \neq 0$), the Josephson current is obviously enhanced. Now, its maximum can reach nearly J_0 as shown by the green dash dot dot line. This is because that the additional QDs provide new transport channels for the electrons or Cooper pairs. Constructive interference occurs when the energy levels of the QDs are the same, resulting in the enhancement of the current [25,35]. The impact of the constructive interference is further strengthened by increasing t_2 . In T-shaped double QDs, however, the inter-dot coupling will weaken the the Josephson current [25]. The perfect constructive interference effect is destroyed by the level detuning δ as shown in Figure 3b, in which the magnitude of J is obviously suppressed. This is the common case in previous double- or triple-QD structures [25,34–37].

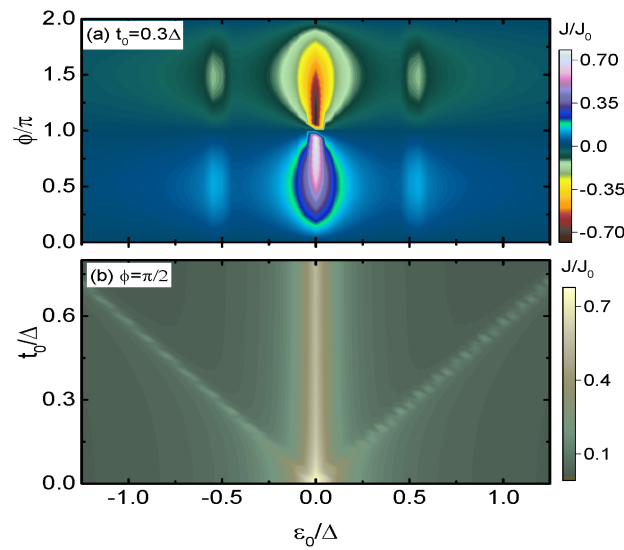


Figure 2. Contour plots of the Josephson currents J as a function of (ϵ_0, ϕ) in (a), and (ϵ_0, t_0) in (b). Other parameters are indicated in the figures.

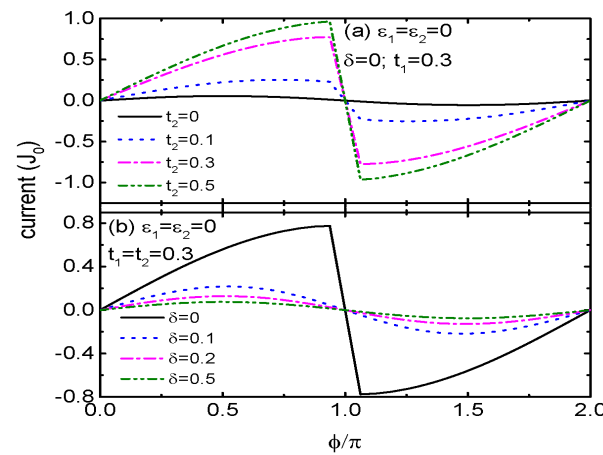


Figure 3. Josephson current J as a function of phase bias ϕ for various t_2 in (a), and different δ in (b) for the indicated parameters.

3.2. Variation of J_c with ϵ_1 for Different ϵ_2, t_2 and δ

Figure 4 shows the relationship between critical current J_c and ϵ_1 for different values of ϵ_2 . First of all, there is only one resonant peak in J_c regardless of the value of ϵ_2 , and the position of the peak depends on the value of ϵ_2 in a nonlinear way. For $\epsilon_2 = 0$, the peak in J_c is centered at $\epsilon_1 = 0$ as indicated by the black solid line in Figure 4a. It is then shifted to the negative regime of $\epsilon_1 < 0$ for $0 < \epsilon_2 < 0.4\Delta$, as shown in Figure 4a. Meanwhile, the peak's height is obviously lowered. For $\epsilon_2 = 0.4\Delta$, as is indicated by the green dash dot dot line, the peak moves back to the position of $\epsilon_1 = 0$, and becomes to be very wide. With even increasing $\epsilon_2 > 0.4\Delta$, the peak is shift to the regime of $\epsilon_1 > 0$. For the case of $\epsilon_2 < 0$, the peak in J_c undergoes similar changes as that of $\epsilon_2 > 0$. The peak's positions for positive and negative ϵ_2 are totally mirror symmetric with respect to $\epsilon_1 = 0$. In double or triple QDs systems, the position of the peak in J_c will remain at the negative or positive ϵ_1 regime depending on the sign of ϵ_2 , and is very different from the present case [25,35]. We attribute this result to the complex quantum interference effect in the present quadruple QDs device [40].

The impacts of t_2 and levels' detuning δ between QDs 3 and 4 are displayed in Figure 5 for fixed $\epsilon_2 = 0.3\Delta$. For $t_2 = 0.3\Delta$, as indicated by the blue triangle line in Figure 5a, the peak in J_c emerges at about $\epsilon_1 = -0.3\Delta$, which corresponds to the blue dot line in Figure 4a.

When $t_2 = 0$, QD2 is decoupled from QDs 3 and 4 and the present system becomes a T-shaped double QDs. Now the peak in J_c emerges whenever $\varepsilon_1\varepsilon_2 = t_1^2$ [25]. For the chosen parameters $t_1 = \varepsilon_2 = 0.3\Delta$, J_c develops a peak at $\varepsilon_1 = \Delta/3$ as indicated by the black square line in Figure 5a. For a small value of $t_2 = 0.1\Delta$, the position of the peak in J_c moves toward larger positive value of ε_1 , and then is shifted to a negative ε_1 by an increased t_2 as shown by the blue triangle and pink inverted triangle lines in Figure 5a. These results are in consistent with those shown in Figure 4, which is arisen from fact that the quantum interference effect from QDs 3 and 4 will change the critical Josephson current in a complex way. As is indicated by the blue triangle line in Figure 5b, the critical current develops a peak around $\varepsilon_1 = -0.3\Delta$ for the case of $\delta = 0$. The peak position then is monotonously shifted toward the positive ε_1 regime with increasing δ , accompanied by an increased in height. Accordingly, the critical current is adjustable by changing the energy levels of dots 3 and 4 that are not directly coupled to QD1.

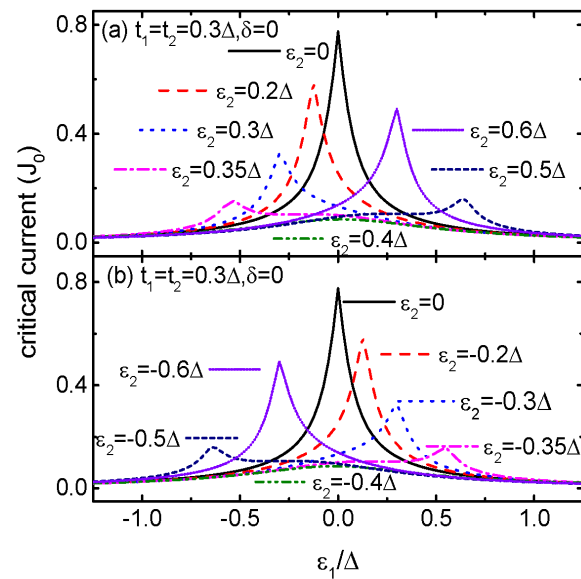


Figure 4. Critical Josephson current J_c as a function of energy level of QD1 for positive ε_2 in (a), and negative ε_2 in (b) for the indicated parameters.

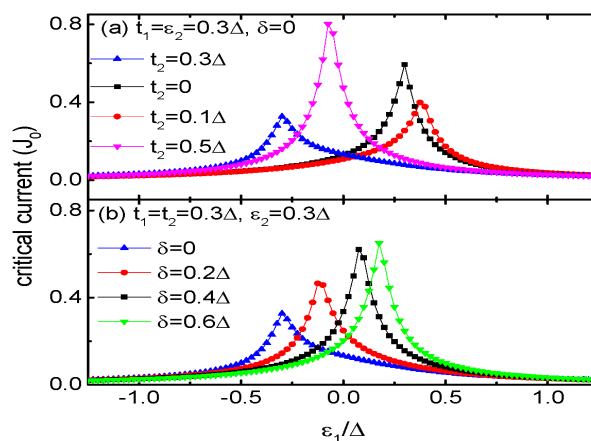


Figure 5. Josephson current as a function of ε_1 for fixed $\varepsilon_2 = t_1 = 0.3\Delta$ and different t_2 in (a), different δ in (b) for the indicated parameters.

3.3. Fano Resonances in $J_c \sim \varepsilon_2$ for Different ε_1, t_2 and δ

We now show the Fano resonances in the curve of $J_c \sim \varepsilon_2$ in Figure 6. When the QDs are coupled to each other by the same amplitudes $t_1 = t_2 = 0.3\Delta$ and $\delta = 0$, the critical current develops a peak at $\varepsilon_2 = 0$ and two valleys around $\pm\sqrt{t_1^2 + t_2^2}$ under the condition

of $\varepsilon_1 = 0$ as indicated by the black solid line. When the energy level of QD1 is shifted away from the Fermi level ($\varepsilon_1 \neq 0$), two asymmetric peaks emerge individually at positive and negative ε_2 regimes. Interestingly, the valleys at $\pm\sqrt{2}t_2$ remains unchanged regardless of the values of either ε_1 or t_1 (except for the case of $t_1 = 0$). The $J_c \sim \varepsilon_2$ curve now shows the typical Fano lineshape, which is similar to the case in T-shape double QDs [25]. Different from the results in ref. [25] in which there is one Fano resonance and one valley, there are two Fano resonances and two valleys in the present quadruple QDs molecule. Moreover, the critical current satisfies the relation of $J_c(\varepsilon_1, \varepsilon_2) = J_c(-\varepsilon_1, -\varepsilon_2)$ due to the electron-hole symmetry, a result also found previously in ref. [25].

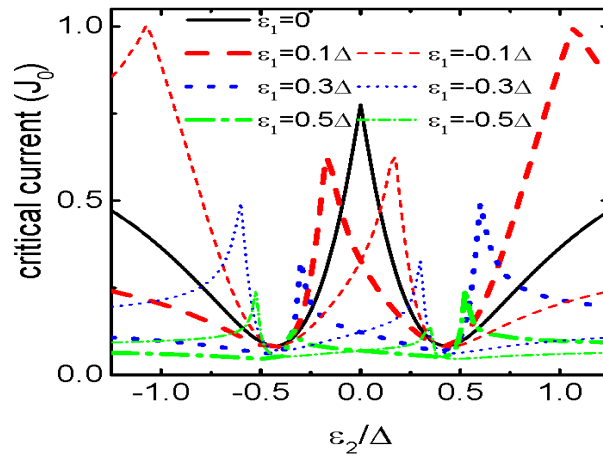


Figure 6. Josephson current as a function of ε_2 for varying ε_1 . Other parameters are $t_1 = t_2 = 0.3\Delta$ and $\delta = 0$.

Finally we examine the influences of t_2 and δ on the critical current in Figure 7. For $t_2 = 0$, there is one Fano resonance positioned at $\varepsilon_2 = t_1^2/\varepsilon_1$ and one valley at $\varepsilon_2 = 0$, which has been found in ref. [25]. For nonzero t_2 as shown in Figure 7a, another pair of Fano resonance and valley emerge due to the opening of two new transport channels through QDs 3 and 4, respectively. With increasing t_2 , the Fano resonance and valley at $\varepsilon_2 > 0$ and $\varepsilon_2 < 0$ are shift individually to higher and lower dot level regimes, respectively. In Figure 7b, one finds that there are three pairs of Fano resonances and valleys in the curve of $J_c \sim \varepsilon_2$ when the energy levels of QDs 3 and 4 are different from each other ($\delta \neq 0$). This is because now the transport channels through QDs 3 and 4 are not identical and thus induces the Fano effect [40]. Such a result is also very different from the cases in double or triple QDs systems, and can be used for manipulating the Josephson current.

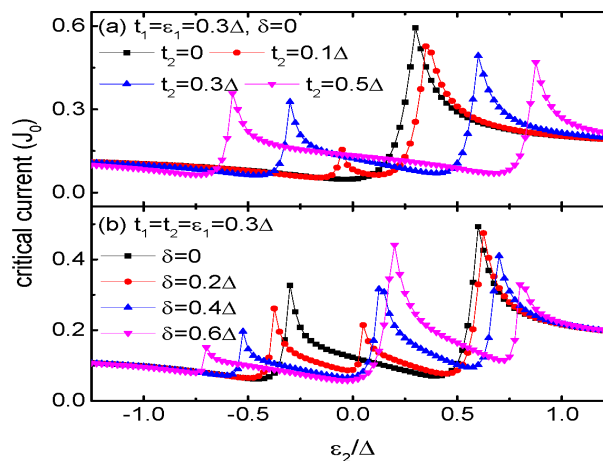


Figure 7. Josephson current as a function of ε_2 for fixed $\varepsilon_1 = t_1 = 0.3\Delta$ and different t_2 in (a), different δ in (b) for the indicated parameters.

4. Summary

In summary, we have studied theoretically the Josephson effect in a quadruple-QDs system sandwiched between superconductor leads. It is assumed that only one QD denoted by QD1 is directly coupled to the leads. We find the coexistence of Dicke and Fano resonances displayed individually in the Josephson current and its critical one. For identical energy levels of the QDs, the Josephson current can be significantly enhanced by the constructive quantum interference arising from the inter-dot couplings. The critical current varying as a function of the energy level of QD1 develops a single resonance peak, whose position can be shifted to either positive or negative energy regimes by changing the energy level of the QDs side-coupled to QD1, as well as the inter-dot coupling strengths. We also find that there are two Fano resonances and valleys in the curve of the critical current varying with respect to the energy level of the side-coupled QDs. Additional Fano resonance and the associated valley emerge when the energy levels of the side-coupled QDs are different from each other. These results are quite different from those in structures with double or triple QDs. Moreover, the critical current satisfies the mirror symmetric relationship with respect to the Fermi level in the superconductor leads due to the electron-hole symmetry, which is similar to the case in the system of T-shaped double QDs. Finally, we note that although the present structure is rather complicated as is compared to those widely studied ones with less QDs, it may provide relatively high values of critical current and high reproducibility of the system parameters, which are the key requirements for utilization in nanoscale digital superconducting technology [51]. The variable QDs' energy levels as well as the interdot couplings can serve as configurable parameters of individual elements and connections between them. This is crucial in development of superconducting quantum circuits for a new generation of quantum processors [52].

Author Contributions: Conceptualization, Formal analysis, Investigation, Writing—original draft preparation, Y.G., Y.S. and F.C.; Formal analysis, Software, Y.G., Y.S. and F.C.; Conceptualization, Writing review and editing, F.C., Z.Y. and L.L. All authors have read and agreed to the published version of the manuscript.

Funding: This research was funded by the Education Science Planning Project of the Department of Education in Guang-dong Province (No. 2023GXJK542), the Educational Quality Project of the Department of Education in Guang-dong Province of China (No. SJD202302), the Innovation Team of Colleges and Universities in Guangdong Province (Grant No. 2021KCXTD040), Guangdong Province Education Department (Grant No. 2023KTSCX174), the Key Laboratory of Guangdong Higher Education Institutes (Grant No. 2023KSYS011), and Science and Technology Bureau of Zhongshan (Grant No. 2023B2035).

Institutional Review Board Statement: Not applicable.

Informed Consent Statement: Not applicable.

Data Availability Statement: All data included in this study are available upon request by contact with the corresponding author.

Conflicts of Interest: The authors declare no conflicts of interest.

References

1. Josephson, B.D. Possible new effects in superconductive tunnelling. *Phys. Lett.* **1962**, *1*, 251. [[CrossRef](#)]
2. Josephson, B.D. The discovery of tunnelling supercurrents. *Rev. Mod. Phys.* **1974**, *46*, 251. [[CrossRef](#)]
3. Tafuri, F. (Ed.) *Fundamentals and Frontiers of the Josephson Effect*; Springer Series in Materials Science; Springer Nature: Berlin/Heidelberg, Germany, 2019; Volume 286, ISBN 978-3-030-20724-3. [[CrossRef](#)]
4. Makhlin, Y.; Schön, G.; Shnirman, A. Quantum-state engineering with Josephson-junction devices. *Rev. Mod. Phys.* **2001**, *73*, 357. [[CrossRef](#)]
5. Pal, B.; Chakraborty, A.; Sivakumar, P.K.; Davydova, M.; Gopi, A.K.; Pandeya, A.K.; Krieger, J.A.; Zhang, Y.; Date, M.; Ju, S.; et al. Josephson diode effect from Cooper pair momentum in a topological semimetal. *Nat. Phys.* **2022**, *18*, 1228. [[CrossRef](#)] [[PubMed](#)]
6. Amundsen, M.; Linder, J.; Robinson, J.W.A.; Žutić, I.; Banerjee, N. Colloquium: Spin-orbit effects in superconducting hybrid structures. *Rev. Mod. Phys.* **2024**, *96*, 021003. [[CrossRef](#)]
7. Martín-Rodero, A.; Yeyati, A.L. Josephson and Andreev transport through quantum dots. *Adv. Phys.* **2011**, *60*, 899. [[CrossRef](#)]

8. Zwolak, J.P.; Taylor, J.M. Colloquium: Advances in automation of quantum dot devices control. *Rev. Mod. Phys.* **2023**, *95*, 011006. [[CrossRef](#)]
9. Kastner, M.A. Artificial Atoms. *Phys. Today* **1993**, *46*, 24. [[CrossRef](#)]
10. Glazman, L.; Raikh, M. Resonant Kondo transparency of a barrier with quasilocal impurity states. *JETP Lett.* **1988**, *47*, 452. <http://jetpletters.ru/ps/1095/article-16538.shtml>.
11. Newns, D.M.; Read, N. Mean-field theory of intermediate valence/heavy fermion systems. *Adv. Phys.* **1987**, *36*, 799. [[CrossRef](#)]
12. Sun, Q.F.; Wang, J.; Lin, T.H. Photon-assisted andreev tunneling through a mesoscopic hybrid system. *Phys. Rev. B* **1999**, *59*, 13126. [[CrossRef](#)]
13. Sun, Q.F.; Wang, J.; Lin, T.H. Control of the supercurrent in a mesoscopic four-terminal Josephson junction. *Phys. Rev. B* **2000**, *62*, 648. [[CrossRef](#)]
14. Zhu, Y.; Sun, Q.F.; Lin, T.H. Andreev bound states and the π -junction transition in a superconductor/quantum-dot/superconductor system. *J. Phys. Condens. Matter* **2001**, *13*, 8783. [[CrossRef](#)]
15. Buitelaar, M.R.; Nussbaumer, T.; Schönenberger, C. Quantum Dot in the Kondo Regime Coupled to Superconductors. *Phys. Rev. Lett.* **2002**, *89*, 256801. [[CrossRef](#)] [[PubMed](#)]
16. Sun, Y.F.; Mao, Y.; Sun, Q.F. Design of Josephson diode based on magnetic impurity. *Phys. Rev. B* **2023**, *108*, 214519. [[CrossRef](#)]
17. Mao, Y.; Yan, Q.; Zhuang, Y.C.; Sun, Q.F. Universal Spin Superconducting Diode Effect from Spin-Orbit Coupling. *Phys. Rev. Lett.* **2024**, *132*, 216001. [[CrossRef](#)]
18. Debnath, D.; Dutta, P. Gate-tunable Josephson diode effect in Rashba spin-orbit coupled quantum dot junctions. *Phys. Rev. B* **2024**, *109*, 174511. [[CrossRef](#)]
19. Xu, L.T.; Li, X.Q.; Sun, Q.F. Majorana dc Josephson current mediated by a quantum dot. *J. Phys. Condens. Matter* **2017**, *29*, 195301. [[CrossRef](#)]
20. Chi, F.; Jia, Q.S.; Liu, J.; Gao, Q.G.; Yi, Z.C.; Liu, L.M. Enhancement of the Josephson Current in a Quantum Dot Connected to Majorana Nanowires. *Nanomaterials* **2023**, *13*, 1482. [[CrossRef](#)]
21. Gao, Y.M.; Zhang, X.Y. Tunable Josephson Current through a Semiconductor Quantum Dot Hybridized to Majorana Trijunction. *Coatings* **2023**, *13*, 1627. [[CrossRef](#)]
22. Pan, H.; Lin, T.H. Control of the supercurrent through a parallel-coupled double quantum dot system. *Phys. Rev. B* **2006**, *74*, 235312. [1103/PhysRevB.74.235312](https://doi.org/10.1103/PhysRevB.74.235312). [[CrossRef](#)]
23. Pan, H.; Lin, T.H. Tunable supercurrent in a parallel double quantum dot system. *Eur. Phys. J. B* **2007**, *57*, 299. [[CrossRef](#)]
24. Pan, H.; Cui, Y.M.; Wang, H.L.; Wang, R.M. Spin-polarized Andreev reflection and spin accumulation in a quantum-dot Aharonov-Bohm interferometer with spin-orbit interaction effects. *J. Appl. Phys.* **2011**, *110*, 033706. [[CrossRef](#)]
25. Cheng, S.G.; Sun, Q.F. Josephson current transport through T-shaped double quantum dots. *J. Phys. Condens. Matter* **2008**, *20*, 505202. [[CrossRef](#)]
26. Hofstetter, L.; Csonka, S.; Nygård, J.; Schönenberger, C. Cooper pair splitter realized in a two-quantum-dot Y-junction. *Nature* **2009**, *461*, 960. [[CrossRef](#)]
27. Droste, S.; Andergassen, S.; Splettstoesser, J. Josephson current through interacting double quantum dots with spin-orbit coupling. *J. Phys. Condens. Matter* **2012**, *24*, 415301. [[CrossRef](#)] [[PubMed](#)]
28. Nian, L.L.; Zhang, L.; Tang, F.R.; Xue, L.P.; Zhang, R.; Bai, L. Spin-resolved Andreev transport through a double quantum-dot system: Role of the Rashba spin-orbit interaction. *J. Appl. Phys.* **2014**, *115*, 213704... [[CrossRef](#)]
29. Zhang, H.R.; Sun, L.L.; Liu, J. Josephson dc Current through T-Shaped Double-Quantum-Dots Hybridized to Majorana Nanowires. *Coatings* **2023**, *13*, 523. [[CrossRef](#)]
30. Deacon, R.S.; Oiwa, A.; Sailer, J.; Baba, S.; Kanai, Y.; Shibata, K.; Hirakawa, K.; Tarucha, S. Cooper pair splitting in parallel quantum dot Josephson junctions. *Nat. Commun.* **2015**, *6*, 7446. [[CrossRef](#)] [[PubMed](#)]
31. Debbarma, R.; Aspegren, M.; Boström, F.V.; Lehmann, S.; Dick, K.; Thelander, C. Josephson Current via Spin and Orbital States of a Tunable Double Quantum Dot. *Phys. Rev. B* **2022**, *106*, L180507. [[CrossRef](#)]
32. Debbarma, R.; Tsintzis, A.; Aspegren, M.; Souto, R.S.; Lehmann, S.; Dick, K.; Leijnse, M.; Thelander, C. Josephson Junction $\pi - 0$ Transition Induced by Orbital Hybridization in a Double Quantum Dot. *Phys. Rev. Lett.* **2023**, *131*, 256001. [[CrossRef](#)]
33. Gao, Y.M.; Xiao, H.; Jiang, M.H.; Chi, F.; Yi, Z.C.; Liu, L.M. Josephson Diode Effect in Parallel-Coupled Double-Quantum Dots Connected to Unalike Majorana Nanowires. *Nanomaterials* **2024**, *14*, 1251. [[CrossRef](#)]
34. Zhong, S.R.; Jin, L.H.; Yang, C.J.; Li, X.S.; Yi, G.Y. Josephson Effect in a T-Shaped Triple-Quantum-Dot Structure: π -Junction Behavior and Two-Stage Kondo Effect. *Phys. Status Solidi B* **2020**, *257*, 1900568. [[CrossRef](#)]
35. Wang, X.Q.; Yi, G.Y.; Gong, W.J. Dicke-Josephson effect in a cross-typed triple-quantum-dot junction. *Solid State Communi.* **2016**, *247*, 12. [[CrossRef](#)]
36. Bai, L.; Jiang, L.; Zhang, Z.Z.; Duan, C.L. Tunable Josephson current in a lateral triple quantum dot molecule. *J. Appl. Phys.* **2010**, *108*, 123714. [[CrossRef](#)]
37. Bai, L.; Zhang, Q.; Jiang, L.; Zhang, Z.; Shen, R. Tunable supercurrent in a triangular triple quantum dot system. *Phys. Lett. A* **2010**, *374*, 2584. [[CrossRef](#)]
38. Yi, G.; Li, Z.; Chen, X.; Wu, H.; Gong, W.J. Persistent current driven by the Josephson effect in a triple-quantum-dot ring with superconducting leads. *Phys. Rev. B* **2013**, *87*, 195442. [[CrossRef](#)]

39. Yi, G.Y.; Wang, X.Q.; Gong, W.J.; Wu, H.N.; Chen, X.H. Josephson effect in a triple-quantum-dot ring with one dot coupled to superconductors: Numerical renormalization group calculations. *Phys. Lett. A* **2016**, *380*, 1385. [[CrossRef](#)]
40. Ramos-Andrade, J.P.; Pena, F.J.; Gonzalez, A.; Avalos-Ovando, O.; Orellana, P.A. Spin-Seebeck effect and spin polarization in a multiple quantum dot molecule. *Phys. Rev. B* **2017**, *96*, 165413. [[CrossRef](#)]
41. Orellana, P.A.; Ladron de Guevara, M.L.; Claro, F. Controlling Fano and Dicke effects via a magnetic flux in a two-site Anderson model. *Phys. Rev. B* **2004**, *70*, 233315. [[CrossRef](#)]
42. Orellana, P.A.; Lara, G.A.; Anda, E.V. Kondo and Dicke effect in quantum dots side coupled to a quantum wire. *Phys. Rev. B* **2006**, *74*, 193315. [[CrossRef](#)]
43. Trocha, P.; Barnas, J. Kondo-Dicke resonances in electronic transport through triple quantum dots. *Phys. Rev. B* **2008**, *78*, 075424. [[CrossRef](#)]
44. Wang, Q.; Xie, H.Q.; Nie, Y.H.; Ren, W. Enhancement of thermoelectric efficiency in triple quantum dots by the Dicke effect. *Phys. Rev. B* **2013**, *87*, 075102. [[CrossRef](#)]
45. Glodzik, S.; Wojcik, K.P.; Weymann, I.; Domanski, T. Interplay between electron pairing and Dicke effect in triple quantum dot structures. *Phys. Rev. B* **2017**, *95*, 125419. [[CrossRef](#)]
46. Kulik, I.O.; Omelyanchuk, A.N. Properties of superconducting microbridges in the pure limit. *Sov. J. Low Temp. Phys.* **1977**, *3*, 7
47. Dvir, T.; Wang, G.; van Loo, N.; Liu, C.X.; Mazur, G.P.; Bordin, A.; Ten Haaf, S.L.; Wang, J.Y.; van Driel, D.; Zatelli, F.; et al. Realization of a minimal Kitaev chain in coupled quantum dots. *Nature* **2023**, *614*, 445. [[CrossRef](#)]
48. Zhu, Y.; Sun, Q.F.; Lin, T.H. Andreev reflection through a quantum dot coupled with two ferromagnets and a superconductor. *Phys. Rev. B* **2001**, *65*, 024516. [[CrossRef](#)]
49. Ozaeta, A.; Vasenko, A.S.; Hekking, F.W.J.; Bergeret, F.S. Andreev current enhancement and subgap conductance of superconducting FSN hybrid structures in the presence of a small spin-splitting magnetic field. *Phys. Rev. B* **2012**, *86*, 060509(R). [[CrossRef](#)]
50. Golubov, A.A.; Kupriyanov, M.Y.; Ilichev, E. The current-phase relation in Josephson junctions. *Rev. Mod. Phys.* **2004**, *76*, 411. [[CrossRef](#)]
51. Soloviev, I.I.; Bakurskiy, S.V.; Ruzhickiy, V.I.; Klenov, N.V.; Kupriyanov, M.Y.; Golubov, A.A.; Skryabina, O.V.; Stolyarov, V.S. Miniaturization of Josephson Junctions for Digital Superconducting Circuits. *Phys. Rev. Appl.* **2021**, *16*, 044060. [[CrossRef](#)]
52. Vozhakov, V.A.; Bastrakova, M.V.; Klenov, N.V.; Soloviev, I.I.; Pogosov, W.V.; Babukhin, D.V.; Zhukov, A.A.; Satanin, A.M. State control in superconducting quantum processors. *Phys. Uspekhi* **2022**, *65*, 421. [[CrossRef](#)]

Disclaimer/Publisher's Note: The statements, opinions and data contained in all publications are solely those of the individual author(s) and contributor(s) and not of MDPI and/or the editor(s). MDPI and/or the editor(s) disclaim responsibility for any injury to people or property resulting from any ideas, methods, instructions or products referred to in the content.